doi:10.1038/nature10904

1 Supplementary Experiments

Substrate Dependence

To control for substrate effects, the electron energy loss experiment was repeated using 8 nm-thick SiO_2 substrates, purchased from Ted Pella, Inc. Owing to the silica's thickness, signal from the smallest particles underwent greater attenuation compared to the signal on ultrathin carbon. However, strong EELS signals could still be collected from particles ranging from 20 nm down to 3 nm in diameter.

Experimental results are presented in Supplementary Figure 1 and compared with our analytic quantum model. As seen, the trend of plasmon resonances on the SiO_2 substrate closely matches that observed with the carbon: the largest particles exhibit a surface resonance at approximately 3.35 eV and the smallest particles display plasmon resonances at 3.75 eV. These results indicate that the quantum mechanical nature of the LSPR resonances is maintained, independent of substrate.

The particles on the SiO_2 exhibit slightly ($\sim$0.05 eV) higher plasmon resonance frequencies compared to those on carbon. This may be attributed to the silica's lower refractive index ($n = 1.5$ versus amorphous carbon's $n = 2$ [1]), which reduces the overall effective medium index. Indeed, finite-difference time-domain simulations indicate that the overall redshift caused by the SiO_2 substrate is approximately 0.03 eV smaller than that for carbon.

Comparison of EELS and Optical Spectroscopy

When excited optically, the LSPRs of silver spheres smaller than 20 nm in diameter are dominated by the dipole resonance, which is typically three to four orders of magnitude greater in intensity than that of the quadrupole (the first higher order term). For this reason, the quasistatic approximation, which describes these particles as dipoles, is often employed in this size range.

In contrast to optical excitation, EELS techniques can more efficiently excite higher order surface modes, even for sub-20 nm particles. Using the equations of Ferrell et al. [2], we have calculated the electron energy-loss spectra of 10, 20 and 40 nm diameter silver spheres, including the dipolar and quadrupolar modes. The particles' purely dipolar resonance, as generated by the optical quasistatic approximation, is given for comparison. In Supplementary Figure 2a, an effective medium of $n = 1.3$ is used (as it was employed in our study) while in Supplementary Figure 2b, $n = 1.0$ is used (to represent vacuum).

In both figures, the contribution of the quadrupolar resonance is apparent. When the particle is in vacuum, the quadrupole merely acts to broaden the dipole peak. In a medium with $n = 1.3$, the quadrupolar and dipolar peaks of the particle are resolvable in theory, with an energy separation of 0.2 eV (about twice the energy separation that can be resolved with our EELS system). However, the ratio of the quadrupolar peak to the dipolar peak is 0.25. This significant intensity difference precludes experimental observation of these higher order terms with our setup. Note that for particles smaller than 20 nm in diameter, the ratio of the dipolar peak to the quadrupolar peak remains constant within approximately one percent. The ratio does increase for particles larger than 20 nm, which were not investigated in this study.

For these reasons, the EELS resonances detected in our experiment can be compared to optical theory and applied to optical studies involving particles in the 2-20 nm size regime.

2 Supplementary Theory

Analytical Quantum Model

To model the optical properties of quantum-sized plasmonic particles, a revised expression for the permittivity is required. In our analysis, the standard Drude model is recast with Lorentzian terms that are defined quantum mechanically. Classically, Lorentzian terms can be added to the Drude expression to account for the nearly-free nature of electrons in the bulk metal. These terms include a set of oscillator resonance frequencies and corresponding weighted strengths unique to each material [3]. In this report, rather than using Lorentzians to fit the bulk data [4], we employ them to explain the changing dielectric function as particle diameter decreases to the quantum size regime. As will be shown, the nature of the Lorentzian terms is based on fundamental physical phenomena, such as electron transition frequencies and oscillator strengths.

Following the example of Genzel [5] and Kraus [6], the relevant conduction electrons are treated as a free electron gas constrained by infinite potential barriers at the physical edge of the particle. Transition frequencies correspond to the allowed quantum energies of conduction electron transitions from occupied states i within the k-space Fermi sphere to unoccupied states f immediately outside.

The relative magnitude of each of these Lorentzian perturbations is based on the well-established Thomas-Reiche-Kuhn energy-weighted sum rules (also known as the f-sum rules) that are commonly used for absorption processes. Encapsulating significant information about the energy spectrum and eigenfunctions of a system in a compact form, they enabled experimental confirmation of early quantum theory and have since been widely used in solid state physics as well as atomic and nuclear spectroscopy [1]. Here, the technique is employed in the form of oscillator strengths (S_{if}) that correspond to each transition frequency.

The overall permittivity expression can be described as follows:

$$\epsilon(\omega) = \epsilon_{IB} + \omega_p^2 \sum_i \sum_f \frac{S_{if}}{\omega_{if}^2 - \omega^2 - i\gamma\omega}. \tag{1}$$

Here, ϵ_{IB} is a frequency-dependent correction term to account for the contribution of the d-band valence electrons to interband transitions at higher energies. It is constant with particle diameter over the size range of this model, as validated in the literature [7]. The form of ϵ_{IB} is described in later sections of this Supplementary Information.

The plasma frequency, ω_p, is defined as

$$\omega_p = \sqrt{\frac{n_e e^2}{\epsilon_0 M}} \tag{2}$$

where n_e is the volumetric conduction electron density (given 1 electron per atom of silver), e is the elementary charge, ϵ_0 is the permittivity of free space, and M is the mass of the electron. At frequencies below ω_p (9.01 $eV/\hbar$ for silver [3]), a free-electron metal can effectively screen the incident electromagnetic radiation and acts in a reflective manner, but above the plasma frequency, the metal becomes transparent and acts as a dielectric.

The scattering frequency γ is dependent on the nanosphere dimension through the following relation:

$$\gamma = \gamma_{Bulk} + \frac{A v_F}{R} \tag{3}$$

where γ_{Bulk} is an empirical constant for each material ($\gamma_{Bulk} = 0.016\ eV/\hbar$ for silver [5]), R is the particle radius, and v_F is the Fermi velocity of electrons ($\sim 1.4 * 10^6\ m/s$ in silver [8]). A is a fitting coefficient whose value has varied in the literature from 0.1 to 2, depending on the model and experimental system [9, 10, 11, 12]. Here, we use $A = 0.25$, a value based on both single particle experiments and *ab initio* calculations [7, 13].

The frequency of electron transitions from occupied to excited states can be described as

$$\omega_{if} = \frac{E_f - E_i}{\hbar} \tag{4}$$

where the energy levels E_f and E_i depend on the geometry and potential of the system. We assume that the nanocrystal's physical shape closely approximates a sphere (see Figure 1 of the Article) and treat the conduction electrons as particles in an infinite spherical well. The allowed energies are:

$$E = \frac{\hbar^2\pi^2}{8MR^2}(2n + l + 2)^2 \tag{5}$$

where M is the mass of the electron, R is the radius of the sphere, and n and l are the principle and azimuthal quantum numbers, respectively. If we define the excited states' orbital numbers as $n_f = n + \Delta n$ and $l_f = l + \Delta l$, the transition frequencies can be expressed as:

$$\omega_{if} = \frac{\hbar^2\pi^2}{8MR^2}(4n + 2\Delta n + 2l + \Delta l + 4)(2\Delta n + \Delta l). \tag{6}$$

The relative weight of each of these transitions is given by their oscillator strength terms. As dictated by the Thomas-Reiche-Kuhn sum rules, these terms sum to unity and can be described using the standard quantum harmonic oscillator definition

$$S_{if} = \frac{2M\omega_{if}}{\hbar N} |< f|z|i >|^2 \tag{7}$$

where N is the number of conduction electrons in the nanosphere. The matrix element term $< f|z|i >$ is defined as:

$$< f|z|i >= \int \psi^*_{n_f l_f m_f}(r, \theta, \phi) r \cos\theta \psi_{n_i l_i m_i}(r, \theta, \phi) d\tau \tag{8}$$

where ψ_{nlm} represents the wavefunction of a particle in a spherical potential well:

$$\psi_{nlm}(r, \theta, \phi) = j_l(\alpha r) Y_{lm}(\theta, \phi). \tag{9}$$

Here, j_l represents the spherical Bessel function and Y_{lm} represents the standard spherical harmonics. Using the asymptotic approximation for the Bessel function, the wavefunction simplifies to:

$$\psi_{nlm}(r, \theta, \phi) = \frac{2}{R^{1/2}} \frac{\cos\left[\frac{\pi}{2}((2n + l + 2)r/R - (l + 1))\right]}{r} Y_{lm}(\theta, \phi). \tag{10}$$

The electron wavefunction can now be evaluated using spherical harmonic recurrence relations. Using additional simplification and degeneracy considerations described elsewhere [5], the final expression for the oscillator strength is given as:

$$S_{if} \equiv S_{n,l,\Delta n,\Delta l} = \delta_{\Delta l,-1}\frac{16l(2n+2\Delta n+l+1)^2(2n+l+2)^2}{\pi^2 n_F^3(4n+2\Delta n+2l+3)^3(2\Delta n-1)^3} + \delta_{\Delta l,+1}\frac{16(l+1)(2n+2\Delta n+l+3)^2(2n+l+2)^2}{\pi^2 n_F^3(4n+2\Delta n+2l+5)^3(2\Delta n+1)^3} \tag{11}$$

where n_F is the value of the quantum number n on the Fermi surface when $l = 0$. The magnetic quantum number, m, has already been incorporated into the terms and acts as a multiplicative degeneracy factor.

Using equations (2), (3), (6), and (11), the overall permittivity can be described by evaluating equation (1) over the following ranges, as described elsewhere [5]:

$$\begin{aligned} \Delta l &= -1, 1 \\ \frac{1-\Delta l}{2} &\leq \Delta n \leq n_F \\ 0 &\leq n \leq n_F - \frac{1-\Delta l}{2} \\ 2(n_F - n - \Delta n + \frac{1-\Delta l}{2}) &\leq l \leq 2(n_F - n) \end{aligned} \tag{12}$$

The lowest order conduction electron transitions occur when $\Delta n = 1$, while higher order transitions occur in the range $1 < \Delta n \leq n_F$. Interestingly, if only the lowest order transitions are considered in the model, the plasmon resonance trend shows remarkable similarity to that predicted by the *ab initio* DFT model presented in the Article (see Supplementary Figure 3).

Interband Transition Term

While the Drude model effectively describes noble metals at low frequencies, the optical properties of silver diverge for excitation energies greater than ~ 3.8 eV owing to the contribution of interband transitions of d-band valence electrons. To account for this divergence, the basic Drude expression can be supplemented by an additional, frequency-dependent, interband term (ϵ_{IB}):

$$\epsilon(\omega) = \epsilon_{IB} - \frac{\omega_p^2}{\omega^2 + i\gamma\omega} \tag{13}$$

This additional corrective term was fit to the imaginary portion of the literature permittivity data [4] as a sigmoid with the expression:

$$\mathrm{Im}(\epsilon_{IB}) = \frac{3.66}{1 + e^{-(10*(\omega-4.06))}} \tag{14}$$

The corresponding correction to the real portion of the permittivity was calculated through Kramers-Kronig consistency [14].

Including these interband contributions, the Drude model agrees with literature permittivity data [4] across near-infrared and ultraviolet frequencies (1-5 eV) to within 5%, as seen in Supplementary Figure 4. This permittivity model can be used to accurately predict the plasmon spectra of classically-sized nanoparticles and agrees well with our large-particle LSPR energy loss spectra of Article Figure 2.

Supplementary References

[1] Palik, E. D. *Handbook of Optical Constants of Solids* (Elsevier, San Diego, California, 1998).

[2] Ferrell, T. L. & Echenique, P. M. Generation of surface excitations on dielectric spheres by an external electron beam. *Physical Review Letters* **55**, 1526–1529 (1985).

[3] Rakić, A. D., Djurišić, A. B., Elazar, J. M. & Majewski, M. L. Optical properties of metallic films for vertical-cavity optoelectronic devices. *Applied Optics* **37**, 5271–83 (1998).

[4] Johnson, P. B. & Christy, R. W. Optical constants of the noble metals. *Physical Review B* **6**, 4370–4379 (1972).

[5] Genzel, L., Martin, T. P. & Kreibig, U. Dielectric function and plasma resonances of small metal particles. *Zeitschrift für Physik B* **21**, 339–346 (1975).

[6] Kraus, W. A. & Schatz, G. C. Plasmon resonance broadening in small metal particles. *The Journal of Chemical Physics* **79**, 6130–6139 (1983).

[7] He, Y. & Zeng, T. First-Principles Study and Model of Dielectric Functions of Silver Nanoparticles. *The Journal of Physical Chemistry C* **114**, 18023–18030 (2010).

[8] Kreibig, U. & Fragstein, C. V. The limitation of electron mean free path in small silver particles. *Zeitschrift für Physik* **224**, 307–323 (1969).

[9] Kreibig, U. & Genzel, L. Optical absorption of small metallic particles. *Surface Science* **156**, 678–700 (1985).

[10] Amendola, V. & Meneghetti, M. Size Evaluation of Gold Nanoparticles by UV-vis Spectroscopy. *The Journal of Physical Chemistry C* **113**, 4277–4285 (2009).

[11] Alvarez, M. M. *et al.* Optical Absorption Spectra of Nanocrystal Gold Molecules. *The Journal of Physical Chemistry B* **101**, 3706–3712 (1997).

[12] Hövel, H., Fritz, S., Hilger, A., Kreibig, U. & Vollmer, M. Width of cluster plasmon resonances: bulk dielectric functions and chemical interface damping. *Physical Review B* **48**, 18178–18188 (1993).

[13] Berciaud, S., Cognet, L., Tamarat, P. & Lounis, B. Observation of intrinsic size effects in the optical response of individual gold nanoparticles. *Nano Letters* **5**, 515–8 (2005).

[14] Bohren, C. F. & Huffman, D. R. *Absorption and Scattering of Light by Small Particles* (Wiley-VCH, Weinheim, 1983).

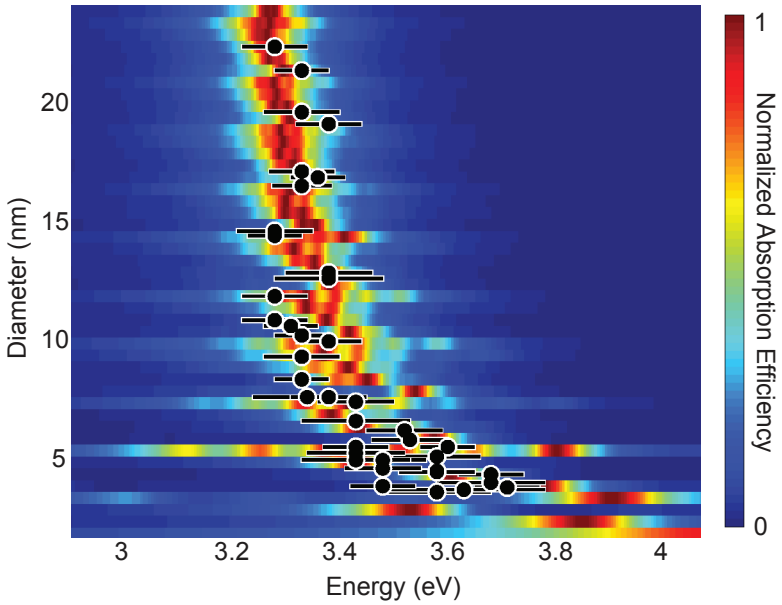

Supplementary Figure 1: Plot of LSPR energies for ligand-free silver spheres on 8 nm-thick SiO_2 TEM substrates (black dots). The energies predicted by the analytic quantum permittivity model are also included on the colourmap, showing excellent agreement. Note that for particles on SiO_2, the experimental peak resonance energies are ∼0.05 eV higher compared to those on carbon. This energy shift is caused by the lower refractive index of the SiO_2 substrate, and accordingly the effective medium index used for the theory is decreased compared to that used for the carbon.

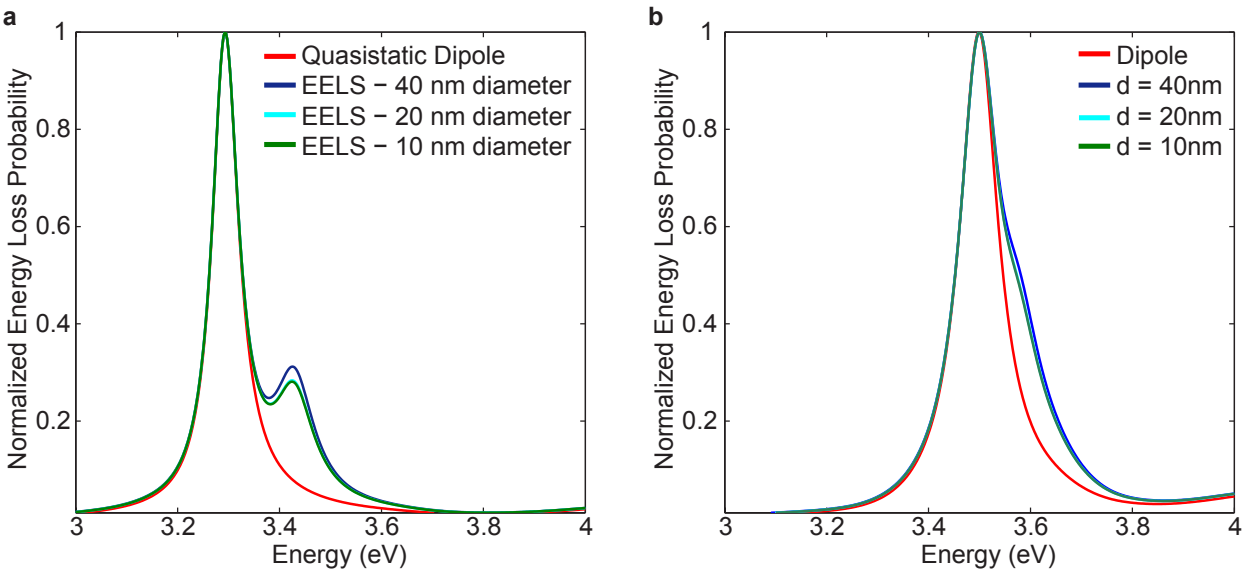

Supplementary Figure 2: Comparison of the theoretical electron energy-loss spectra for silver spheres including dipolar and quadrupolar contributions to that of a pure dipole, as would be generated optically. Results are included for particle diameters of 40, 20, and 10 nm, with nearly-indistinguishable spectra for the 20 and 10 nm particles. Note that retardation effects were not included. An effective medium of $n = 1.3$ is used in (a) and $n = 1.0$ is used in (b). The electron beam, directed immediately outside the particle's edge, is able to excite the quadrupole more strongly than in optical experiments, but the dipole resonance still dominates.

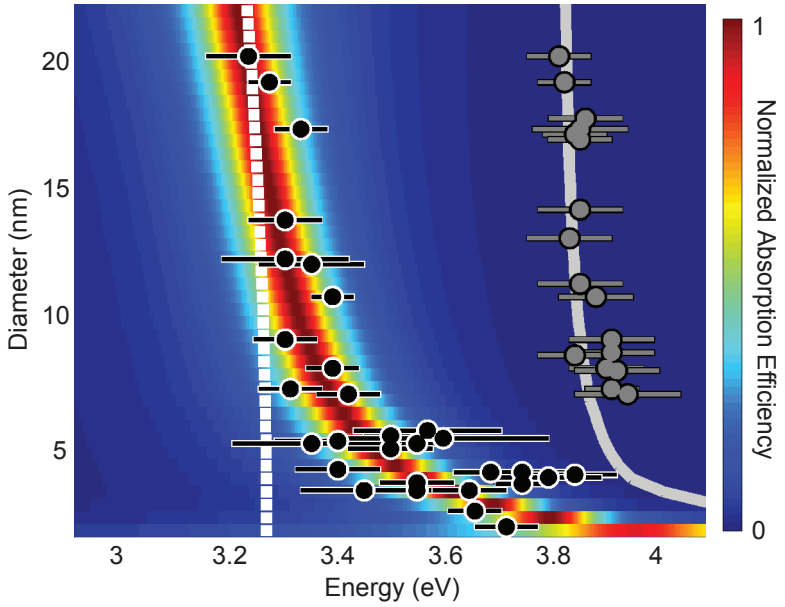

Supplementary Figure 3: Comparison of experimental LSPR energies for various particle diameters (black dots) with the absorption spectra generated from the analytic quantum permittivity model using only the lowest order transitions. The experimental bulk resonance energies are also included (grey dots) along with the theoretical prediction (grey line). Classical Mie theory peak prediction is indicated by the white dashed line.

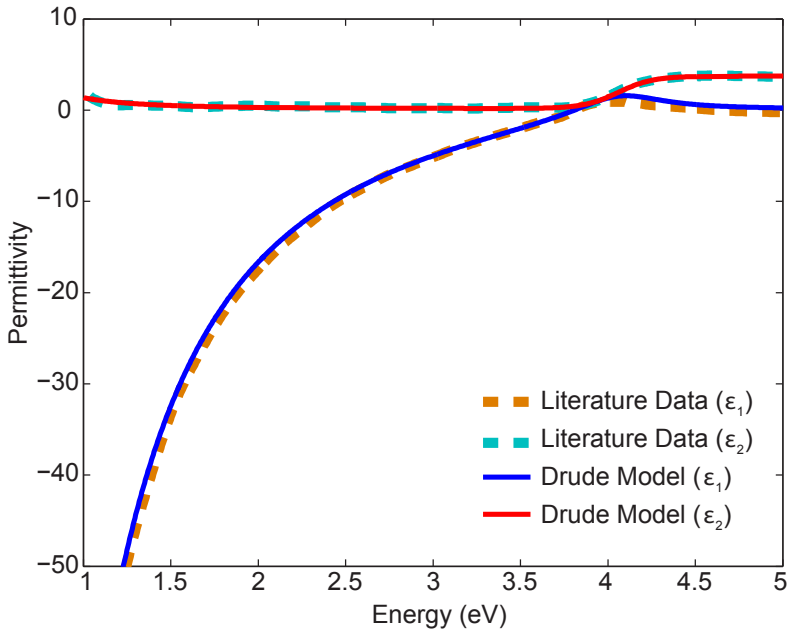

Supplementary Figure 4: The real (ϵ_1) and imaginary (ϵ_2) components of bulk silver permittivity, comparing empirical permittivity data from the literature [4] with the modified Drude fit incorporating interband transitions.